



# Numerical Investigation of the Influence of Microchannel Geometry on the Droplet Generation Process

S. S. S. Paramanantham<sup>1,2</sup>, V. M. Nagulapati<sup>1</sup> and H. Lim<sup>1,3†</sup>

<sup>1</sup>*School of Energy and Chemical Engineering, Ulsan National Institute of Science and Technology, Ulsan – 44919, Republic of Korea*

<sup>2</sup>*Carbon Value Co., Ltd, 2802 A-dong, 97, Centum Jungang-ro, Haeundae-gu, Busan – 48058, Republic of Korea*

<sup>3</sup>*Department of Energy Engineering, Ulsan National Institute of Science and Technology, Ulsan – 44919, Republic of Korea*

†*Corresponding Author Email: [hklm@unist.ac.kr](mailto:hklm@unist.ac.kr)*

(Received February 11, 2022; accepted May 8, 2022)

## ABSTRACT

Two immiscible fluids flowing in microchannels are essential for microdevices to achieve efficient transfer of fluid reactions and heat, droplet mixing, extraction, and emulsification. In this study, a numerical investigation of the flow regime of droplet generation and the droplet breakup behavior of immiscible fluids (water and oil) in various microchannel structures was undertaken. To predict the influence of the microchannel structure on droplet generation and the breakup process, a two-phase level set method was implemented. The generated droplets were validated with experimental results of the T-shape microchannel structure. The obtained numerical results were in good agreement with the experimental results. Furthermore, the validated model was used to investigate the effect of various types of microchannel structures on droplet generation and breakup behavior. Also, the effects of different viscosities, wetted wall contact angles, surface tension, the size of continuous and dispersed channel widths, and the continuous flow rate for droplet generation and breakup in the microchannel were studied. This work contributes to better understanding of effective microchannel design.

**Keywords:** Microfluidics; Immiscible fluids; Two-phase flow; Droplet; Channel structure; Level-set method; Generator and breakup.

## 1. INTRODUCTION

Fast-growing micro-electromechanical systems (MEMS) technology is capable of performing both chemical and biological analyses at just a few micrometers in size using microfluidic chips (Dittrich and Manz 2006; Joanicot and Ajdari 2005; Liu and Zhang 2009). Nowadays, microfluidic systems are being developed for various purposes, including for use in microdroplet technology and microfluidic devices (Shang *et al.* 2017; Zhu and Wang 2017). Generally, microdroplet technology is established in microfluidic devices, where such devices are used to generate tiny liquid droplets. In the microdevice confirmed for droplet generation, the generated droplet processing requires mixing the fluid to generate the droplet (Ba *et al.* 2015), sorting the droplet according to its size and shape (Zhang *et al.* 2009), splitting the droplet to necessary size (Jung *et al.* 2016), merging the different droplet components (Yang *et al.* 2010), and trapping the droplet in a delivery system (Rambach *et al.* 2017). The microdroplet technology is implemented

through various applications such as spray cooling, self-cleaning, and anti-icing, and in the process, droplets make contact with the solid surface directly (Luo *et al.* 2021). Studied applications for this technology include the fields of microreactors, drug delivery systems, cell biology, chemical synthesis, chemical kinetics (Song *et al.* 2003), protein crystallization (H. Chen *et al.* 2005), micro extraction (D. L. Chen *et al.* 2005), various synthesis applications such as organic molecules (Hatakeyama *et al.* 2006), nano particles (Shestopalov *et al.* 2004; Yen *et al.* 2005), bead/particles (Nie *et al.* 2005), chemicals (Shum *et al.* 2009), synthetic biology (Gach *et al.* 2017), and organ-on-a-chip-based COVID treatment (Yang *et al.* 2021).

There are two different major classifications of techniques for generating droplets—namely, active and passive techniques. Generally, an active approach makes it more complicated to control droplet generation because the active system itself contains numerous controlling parameters within a

microdevice. A system operated and controlled by an intrinsic force and external energy, or an additional energy source, is needed. Based on an external source of input to the system, active techniques can be further classified as: electrical, mechanical, electromagnetic, and so on (Chen *et al.* 2007; Zhu and Wang 2017). An intrinsic force approach based on material properties means that droplet generation is controlled via viscosity, interfacial tension, channel wettability, fluid density, and velocity. However, due to external energy, active system design accounting for complexity and control parameters has largely focused on an active-based intrinsic force or a passive approach for microdroplet generation. The use of a passive approach is majorly influenced by fluid viscosity ratios. The principle behind a passive system is that the immiscible fluid, known as the dispersed phase, passes through another fluid called the continuous phase and forms a droplet in the system. Passive approaches are classified according to geometrical configuration, for example, squeezing (Garstecki *et al.* 2005), jetting and dripping (Utada *et al.* 2007; J. Zhang *et al.* 2021), and tip-streaming and tip-multi-breaking (Zhu *et al.* 2015). The squeezing mechanism is dissimilar to other types of passive approaches, since channel restriction plays a vital role in controlling the squeezing reign and inhibits capillary instability so that breakup reveals quasi-static mechanisms up to the final stage of pinch off. In contrast, other types of droplet breakup are based on capillary instability, with the surface tension force reducing the interfacial area needed for the minimum value of interfacial energy to satisfy thermodynamic principles. To avoid deformation, the viscous force and the inertial force act on the liquid interface, and the effect of this reduces the interfacial tension forces. Due to this force behavior, a specific method of droplet breakup is formed and a droplet is generated within the established parameters. Furthermore, the influence of flow rates and capillary number on microdroplet generation in the crossflow of a microdevice have been investigated (Venkateshwarlu and Bharti 2021).

Using a passive approach is a promising way to generate a droplet that can be further classified into three categories, according to: geometrical shape and flow conditions, such as T-junction (Mastiani *et al.* 2017); flow-focusing (Kim *et al.* 2008); and coflowing (Hong and Wang 2007). A T-junction microdevice was reported by Thorsen *et al.* (2001) to generate a monodisperse lower viscous phase droplet (water) in a higher viscous phase (oil). The lattice Boltzmann method has been used to predict droplet size mainly correlated with capillary number and flux in the system (van der Graaf *et al.* 2006). Centrifugal microfluidics–lab-on-a-CD–is a passive technique that generates multiple droplets using a CD platform; it achieves monodisperse droplets simply and quickly. This technique can very precisely control droplet size (Madadelahi *et al.* 2020). Many studies have demonstrated that the width ratio of the continuous phase channel to the dispersed phase channel T-junction, and orifice flow width, have influenced and determined the shape, size, and diameter of droplets (Raj *et al.* 2010; Shi *et*

*al.* 2014; van der Graaf *et al.* 2006). The hydrodynamics interaction-based behavior of droplet-synchronizing flow through a T-junction microchannel controlled by flow conditions of continuous and dispersed was observed (Um *et al.* 2020). Experimental studies for monodisperse droplet generation designed for both low and high capillary numbers using a T-shaped-junction-based microdroplet generator have also been conducted (Zeng *et al.* 2021). New methods to achieve a monodisperse droplet shape were observed experimentally. The continuous phase was considered as a lower viscous phase and the dispersed phase was considered as a higher viscous phase, causing droplet generation to be a balloon shape regime (Tarchichi *et al.* 2013). Furthermore, the sequence of droplet formation in microfluidic networks involves complex behaviors to obtain a simultaneous flow for generating many droplets. A simplified description of the realistic estimation of continuous hemodynamic models and the relevance of the discrete nature of blood to the excitation of oscillations was presented by Cybulski *et al.* (2019). The most comprehensive study of the latest droplet production techniques involve passive and active approaches. The passive mode does not require external power, while the active mode requires external power, such as from an external electric field, a magnetic field, an acoustic field, or a laser field. The formation of the required number of droplets in microfluidics is expected to form an important direction for future research (Han and Chen 2021). The development of machine learning (ML) capabilities have also been explored to try and overcome challenges in microfluidic technology and biomedical and biotechnology applications. The integration of both Droplet Based Microfluidic (DBMF) and ML facilitates the development of high-precision, automated and optimal tools for multiple applications (Srikanth *et al.* 2021). Other aspects of microdroplet interaction occur in proton exchange membrane fuel cells (PEMFCs); their channels see a considerable impact on the wall, and this affects cell performance (Z. Zhang *et al.* 2021).

Achieving continuous production of microdroplets is another area of challenge due to the droplet generation and breakup directly associated with the fluid physical properties. It is dependent on both phases of viscosity, density, flow rate, interfacial tension, and geometrical configuration. Depending on the flow condition and geometrical configuration, generated droplets may vary and experience phenomena such as Taylor bubbles, choke flow, and continuous flow. To avoid flow variation, each condition needs to be verified to obtain the required shape, size, and diameter of droplets. This kind of verification is hard to do experimentally due to the setup fabrication, flow rate control difficulties, system complexity, and expenses of the system. Added to that, research is still in progress to verify which types of configurations obtain an effective generation rate. Some researchers have proposed droplet- or bubble-splitting techniques to increase the generation rate. The approaches are quite complex in terms of geometrical configuration and improving the generation rate and various flow

properties can be verified by using numerical methods instead of a physical test setup. A numerical approach is apt because there is an absence of device complexity and controlling parameters; it is also easy to test different ideas.

Most literature has focused on the T-junction microchannel. In this numerical method, based on two-dimensional (Ngo *et al.* 2015; Sartipzadeh *et al.* 2020), two-phase LSM, involves approaches for analyzing the microchannel under various phenomena using COMSOL 5.6. This study contains mainly two approaches, that is, various configurations of distributor/generator and splitter/breakup. Further investigation was carried out based on flow physics with different viscosities in the continuous phase ( $5e-2-8e-3$  Pa. s), different wetted wall contact angles ( $90-180^\circ$ ), different surface tension ( $4e-3-10e-3$  N/m), different sizes of continuous and dispersed channel width (50 and 100  $\mu\text{m}$ ), and different continuous flow rates (0.2–4 mL/h). In this simulation implemented different geometrical configurations to investigate droplet generation behavior for improving continuous generation and increasing the rate of generation. Geometries such as a T-junction with different geometrical dimensions, L-junction, Y-junction, and inclined dispersed channels with various angles were studied. Moreover, after generating droplets from the distributor, for reducing droplet diameter or increasing droplet growth, a splitter was introduced at the distributor outlet of the microdevice. From the splitter, the droplet split into the required shape and size based on the splitter shape, including V-shape with various angles, needle shape, H-shape, root shape, and M-shape. For achieving the aforementioned shapes and purpose, numerical approaches were implemented so as to be able to study droplet generation and splitting in the microdevice under various geometrical configurations and flow conditions.

## 2. GEOMETRICAL CONFIGURATION

Our microchannel simulation used a T-junction geometry for investigating the breakup and generation rate of droplets in a microdevice. The computational geometrical configuration shown in Fig. 1 and the geometrical dimension are presented as Geometry (Gem) A in Table 1. Gem A had uniform width for both continuous ( $W_c$ ) and dispersed ( $W_d$ ) phases. A two-dimensional model was initially used to validate the experiment (Tarchichi *et al.* 2013; van der Graaf *et al.* 2006). Furthermore, for quantitative analyses of different T-junction dimensions, different types of distributors (Fig. 2) and splitters (Fig. 3) were studied using two-dimensional geometry to reduce the computational time.

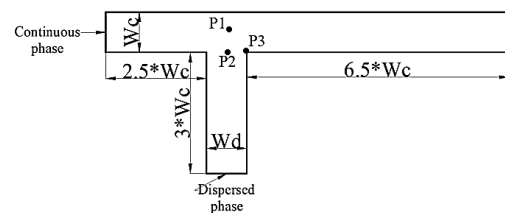


Fig. 1. T-junction microchannel geometry.

Figure 2 shows the different types of distributors for generating the droplet geometry. The geometrical dimension took a uniform width of 100  $\mu\text{m}$  for both phase channels. All the microchannels fell under the principle of capillary instability, with the surface tension force reducing the interfacial area to break up the droplets. The Y-, forward and backward inclined channel webs were considered under different angles of dispersed phase into the continuous phase channel, and the changes of flow channel angle and droplet breakup behavior were investigated.

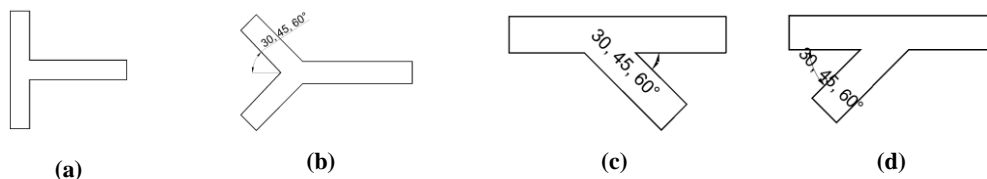


Fig. 2. Geometrical construction of various types of droplet generator/distributor channels: (a) L-junction, (b) Y-junction, (c) backward inclined webs, and (d) forward inclined webs.

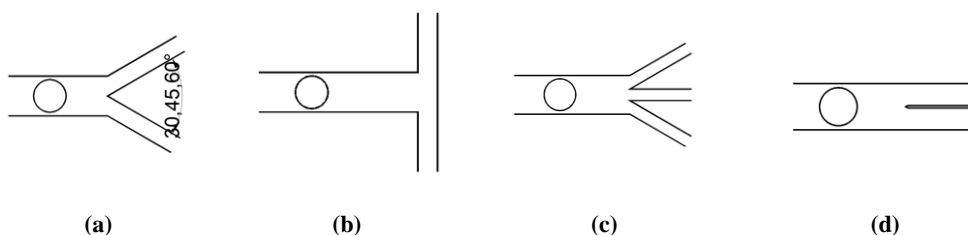


Fig. 3. Geometrical construction of different types of microdroplet splitter channels: (a) V-shaped, (b) H-shaped, (c) M-shaped, and (d) needle splitter.

**Table 1 Geometrical configuration for T-junction**

Geometry	Wc (μm)	Wd (μm)	H (μm)
A	100	100	33
B	100	50	33
C	50	100	33
D	50	50	33
E	100	20	33

Figure 3 shows the different types of droplet splitter geometrical models. Generally, the splitter was used for splitting a droplet after it was generated by the distributor. This approach was fast and produced very tiny droplets; it mainly focused on symmetry dividing the droplet method. The width ratio of the splitting channel and the main channel in all geometrical models was 0.5, except for the M-shaped splitter channel. That had an angle of 30°, and the middle channel width was 3/10 of the main channel width.

### 3. GOVERNING EQUATION

The level set method (LSM) was implemented to investigate droplet generation in a microchannel at different operating conditions. Originally, LSM was derived by Osher and Sethian (1988) and Osher and Fedkiw (1991), and later improved by Olsson and Kreiss (2005). This was the method used in the current investigation. It was intended for a smooth and moving interface between immiscible fluids and denoted as  $\phi$ , when  $\phi = 1$ , and  $\phi = 0$  define the pure phase of continuous and dispersed, respectively,  $1 < \phi > 0$  denoted the interface region or mixture region; however, between  $\phi > 0.5$  and  $\phi < 0.5$ , it was considered to be the mixture fluid of continuous phase and dispersed phase, respectively. In this simulation, an implicit approach of two-phase incompressible Navier–Stokes equation was considered. The incompressible contained continuity (mass conservation) and momentum equations, as follows.

Continuity equation:

$$\nabla \cdot \mathbf{u} = 0 \tag{1}$$

Momentum equation:

$$\rho \frac{\partial \mathbf{u}}{\partial t} + \rho(\mathbf{u} \cdot \nabla)\mathbf{u} = \nabla \cdot \{p\mathbf{I} - \mu[\nabla\mathbf{u} + (\nabla\mathbf{u})^T]\} + \mathbf{F}_{st} + \sigma k \delta \mathbf{n} \tag{2}$$

$$\mathbf{n} = \frac{\nabla\phi}{|\nabla\phi|}, \quad k = \nabla \left( \frac{\nabla\phi}{|\nabla\phi|} \right), \tag{3}$$

$$\delta = 6 \cdot |\nabla\phi| \phi(1 + \phi)$$

where,  $t$ ,  $\mathbf{u}$ ,  $p$ , and  $\mathbf{I}$  are time, velocity vector, pressure, and identity matrix, respectively;  $\sigma$ ,  $k$ ,  $\mathbf{n}$ , and  $\delta$  are surface tension, curvature, unit normal vector, and Dirac delta function, respectively.

The most important problem in the numerical analysis of a moving boundary involves the occurrence of discontinuity in the fluid properties at

the interface. To overcome this, it is important to define the fixed interface thickness wherever flow considerations can be efficiently changed. However, this process might be the source of mass conservation and constant interface thickness issues. A level set function was developed and implemented with a COMSOL Multiphysics® CFD module.

$$\rho \frac{\partial \phi}{\partial t} + \mathbf{u} \cdot \nabla \phi = \gamma \nabla \cdot \left[ -\phi(1 - \phi) \frac{\nabla \phi}{|\nabla \phi|} + \varepsilon \nabla \phi \right] \tag{4}$$

The strong stabilization and reinitialization terms were formed, as in Eq. (4). The moving interface defined in the left side of the equation at the same time as the right side of the equation is accountable for the numerical stabilization and reinitialization, where  $\varepsilon$  denotes interface controlling thickness, and  $\gamma$  denotes the reinitialization term. The  $\mu$  and  $\rho$  are defined dynamic viscosity and density of the fluid, respectively. In this simulation,  $\gamma = 0.05$  m/s and  $\varepsilon = 5e-6$  m.

$$\begin{aligned} \mu &= \mu_c + (\mu_d - \mu_c)\phi \\ \rho &= \rho_c + (\rho_d - \rho_c)\phi \end{aligned} \tag{5}$$

$\rho_c$  and  $\rho_d$  denote density of the continuous and dispersed phases, respectively;  $\mu_c$  and  $\mu_d$  denote viscosity of the continuous and dispersed phases, respectively.

For predicting the effective droplet diameter,  $d$ , an integration operator was applied in the equation for finding the area equivalent to the dispersed phase ( $\phi > 0.5$ ) in Eq. (6).

$$d = 2 \cdot \sqrt[3]{\frac{3}{4\pi} \int_{\Omega} (\phi > 0.5) d\Omega} \tag{6}$$

### 4. NUMERICAL RESULTS AND DISCUSSION

Studies were conducted for microdroplet generation with various physical and flow properties in order to analyze the droplet-generating behavior. Various sizes and structures of microchannel geometry as well as generated droplets split using different types of splitter geometry were also investigated, as detailed in this section.

#### 4.1. Geometrical Model and Validation

The simulation considered the geometrical model of microchannel in order to study droplet breakup and splitting behavior. The computational domain size is displayed in Table 1. The continuous and dispersed phase velocity was considered to be uniform at the inlet, and the outflow was considered to be extrapolation at the outlet. Initially, there was a half-channel–filled dispersed phase in the orthogonal channel; this condition was physically not possible but computationally possible and could avoid numerical instability. In this initial condition, all types of microchannels were considered in this study.

For a grid independence test, the T-junction domain was taken with the flow rate of continuous phase (Qc) = 2 mL/h and dispersed phase (Qd) = 0.2 mL/h.

**Table 2 Physical properties of fluids (Experiment 1; van der Graaf *et al.* 2006).**

Parameters	Continuous phase	Dispersed phase
Viscosity (Pa. s)	1.95e-3	6.71e-3
Density (kg/m <sup>3</sup> )	1e3	1e3
Surface tension (N/m)	5e-3	5e-3
Wetted wall contact angle (Deg)	135	135
Flow rate (mL/h)	0.2 to 4	0.2

The fluid properties are presented in Table 2. Here, we considered the following grid densities: 5330, 37820, and 141140. The comparison of 37820 and 141140 grid numbers has a similar volume fraction, velocity, and pressure profile obtained from points P1, P2, and P3 shown in Fig. 4 (a–d). This assessment gives acceptable convergence over the range of grid densities. Consequently, in this simulation, the droplet breakup and splitter were resolved using 37820 grid densities.

This investigation focused on the formation of droplets in the T-junction microchannel. The dispersed phase from the orthogonal channel met with the continuous phase in the main microchannel to create an immiscible fluid interface. When the dispersed phase penetrated the main channel due to the shearing force of the continuous phase, stretching

of the dispersed phase and volume of the phase increased. Therefore, due to the pressure difference between the phases near the T-junction intersection, it was obtained through the internal pressure gradient in the dispersed phase. Owing to the pressure difference and shear force near the intersection of the T-junction, the dispersed phase lost its thickness. As the interfacial tension of the continuous and dispersed phases was not adequate to withstand the shear force and the pressure difference, the dispersed phase broke up and formed a droplet. The droplet became separated and flowed into the main horizontal channel.

Figure 5 shows the droplet generation based on the above process. During the droplet generation, the following stages were observed: instruction, blocking, squeezing, pinch off, breakup, and droplet. In these stages, the flow condition was heavily influenced by the geometry shape and size. The droplet formation detached physics occurred continuously and a sequence of droplets was formed in the microchannel. However, the size, shape, and droplet frequency differed due to the fluid flow rate of the two phases, geometrical dimension, and fluid physical properties. For investigating the different types of droplet-generating distributors and splitters, the numerical model needed to be verified. Two experimental cases were consequently considered in order to validate the present numerical model.

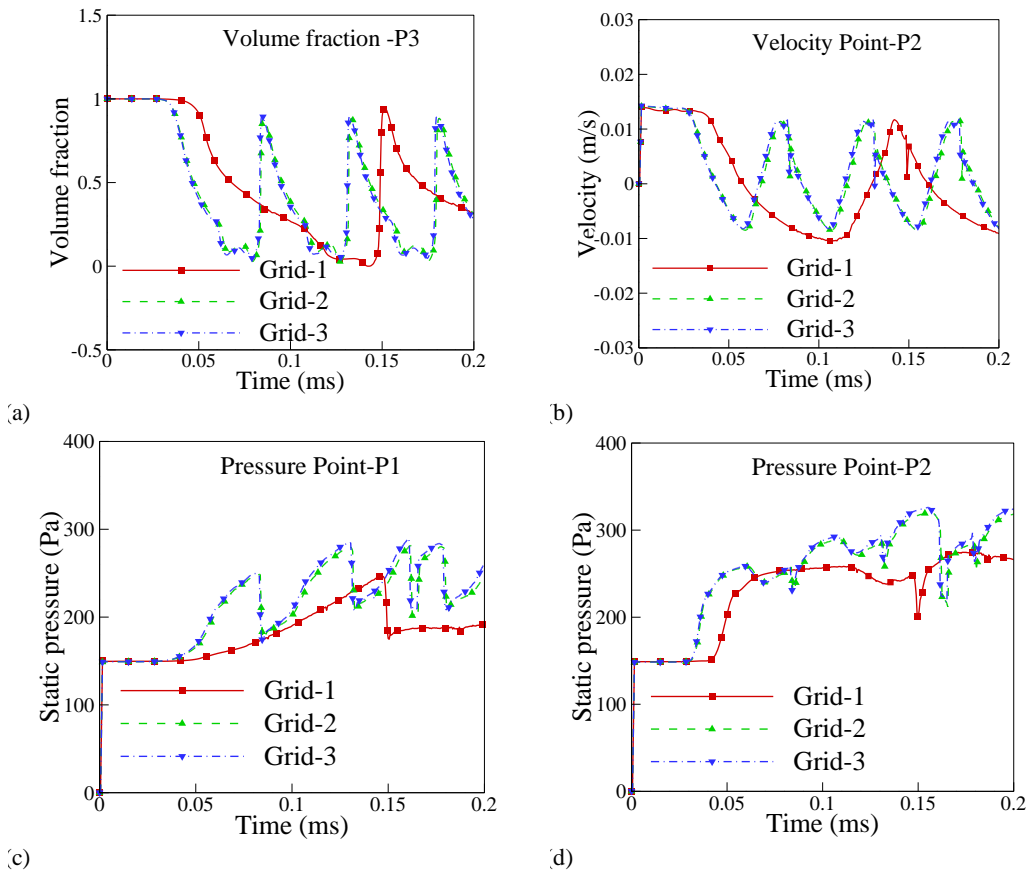


**Fig. 4. Grid independence at location of measuring point P1, P2, and P3: (a) droplet volume fraction at point P3, (b) velocity at point P2, (c) and (d) pressure at points P1 and P2.**

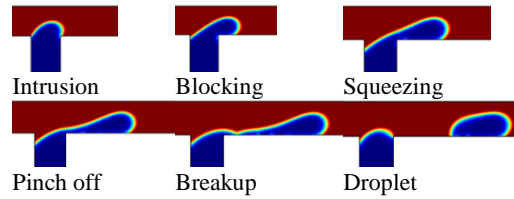
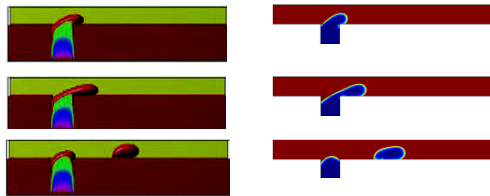


Fig. 5. Stages in the droplet evaluation processes.



Experiment results (van der Graaf *et al.* 2006) Present results

Fig. 6. Comparison of predicted dripping droplet with experimental results and simulation results at the T-junction. Flow rate considered for the continuous phase was 2 mL/h, and dispersed phase was 0.2 mL/h. The comparison reports every  $t = 2.5$  ms using Geometry A (van der Graaf *et al.* 2006).

Figure 6 shows a comparison of dripping droplet generation and breakup with the experimental case. The dripping droplet phenomena occurred when the viscosity ratio of the continuous phase and the dispersed phase was greater than 0.2. The flow rate of the continuous phase was 2 mL/h, the dispersed phase was 0.2 mL/h, and the ratio of the liquid–liquid was 0.1. The dimension of the T-junction width of both phases’ channels were 100  $\mu\text{m}$ . The fluid physical properties are set out in Table 2. When compared with the experimental results, the present numerical results are in good agreement. The droplet generation and breakup were compared with the same time period, showing good agreement between the experiment and the numerical results. The effective droplet diameter,  $d$ , was calculated using Eq. (6).

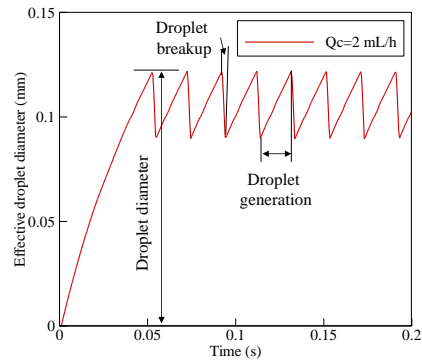


Fig. 7. Effective droplet diameter, droplet generating frequency over time.

Figure 7 illustrates the dispersed phase evolved into continuous phase, which was due to loss of surface tension near the T-junction where the droplet formed. The droplet diameter reached a certain size (0.081 mm) and then the droplet broke up. The first droplet breakup occurred approximately at 0.05 s. However, after that, droplet evolution happened very quickly; the next 0.15 s saw seven droplets. The second droplet occurred within 0.022 s, and the droplet breakup time was 0.002 s, as shown in Fig. 7.

Figure 8 shows the additional validation of droplet breakup for the balloon shape in the T-junction. The flow rate of the continuous phase was 1.2 mm/s, the dispersed phase was 2.1 mm/s, and the ratio of the liquid–liquid was 0.57. The dimension of the T-junction at the continuous phase width was 100  $\mu\text{m}$ , and the dispersed phase channel was 20  $\mu\text{m}$ . The wetted wall contact angle was considered as 180°. The fluid physical properties are defined in Table 3. This regime is based on the balloon droplet. Generally, a balloon droplet occurred when the dispersed phase was a highly viscous fluid. The droplet was created in the continuous phase by the dispersed phase and it assumes the shape of a balloon being blown up. When the balloon formed in a horizontal channel, the intersection of the T-junction near the neck formed. Due to the pressure difference and shear force causing the neck to be thin, the

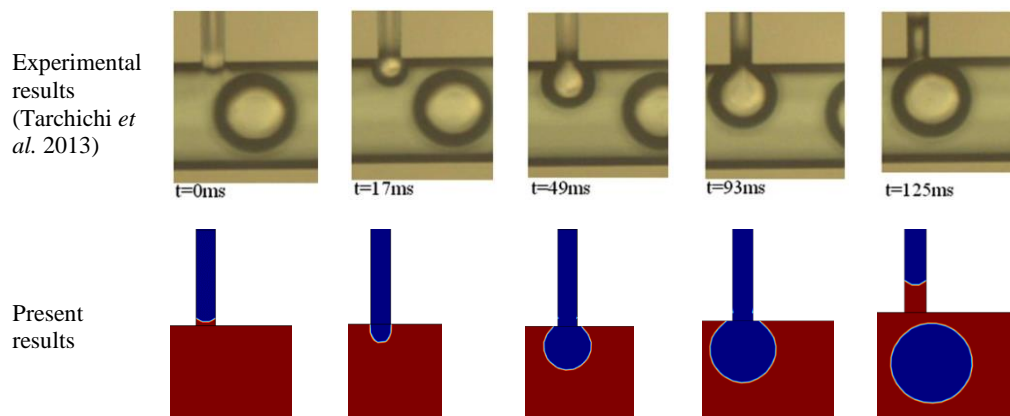


Fig. 8. Comparison of predicted balloon droplet with experimental results and simulation results. The flow rate considered for continuous phase was 1.2 mm/s and dispersed phase was 2.1 mm/s ( $Wc = 100$   $\mu\text{m}$ ; and  $Wd = 20$   $\mu\text{m}$ ; Tarchichi *et al.* 2013).

droplet broke up. The droplet flowed through the main channel. The size of the droplets purely depended on the dispersed phase channel width and droplet frequency based on the continuous phase flow rate (Tarchichi *et al.* 2013). Comparison of the experimental and the present numerical results showed good agreement, as shown in Fig. 9. That figure shows the overlapping comparison experiment and numerical results of droplet size, shape, and distance between droplets. Moreover, the experimental effective droplet diameter was 81  $\mu\text{m}$ , and the present numerical effective droplet diameter was 83  $\mu\text{m}$ . This validation shows good agreement between them.

#### 4.2. Effects of Physical and Fluid Properties

Continuing the validation, it was important to study the behavior of the fluid and physical properties in order to understand the generation behavior while modifying the properties. The following sections discuss the changes of fluid and physical properties in terms of: (1) channel size, (2) flow rate, (3) wetted wall contact angle, and (4) viscosity and surface tension.

##### 4.2.1. Channel size

In another simulation, we considered different widths for both the continuous phase and dispersed phase channels. The channel width assumed two different dimensional values (50 and 100  $\mu\text{m}$ ) to investigate the behavior of droplet formation, as set out in Table 1. For this simulation, changing the geometry dimension and predicting the optimal flow rate to break up the minimum size of the droplet were studied. The rest of the remaining flow and physical properties were set to be constant, as displayed in Table 2. When changing the geometry size, droplet formation could be influenced due to the shear force and pressure before and after the dispersed phase enters into a continuous phase. Depending on the flow rate ratio and the width of the geometry, the droplet size, generation frequency, and droplet shape will be determined. Figure 10 shows the simulation comparison of different dimensions of the T-junction geometry. Here, the optimal flow rate ratio of droplet generation is shown. Thus, each geometry has a different flow rate ratio due to its different geometrical constraint. With the constant continuous phase channel width of 100  $\mu\text{m}$  and by varying the dispersed phase channel widths of 50 and 100  $\mu\text{m}$ , droplet generation increased in the small channel width at the 0.05 flow rate ratio, and droplet frequency increased, as shown in Figs. 10 (a) and 10 (b). Moreover, the droplet size reduced when the dispersed channel width decreased. On the other hand, with increasing flow ratio (0.1) with higher dispersed phase channel width (100  $\mu\text{m}$ ), the droplet size increased, and the generating frequency also increased to twice that of the smaller channel width. Continually, there was a constant width of the continuous phase (50  $\mu\text{m}$ ) and a change in the dispersed phase channel width (50 and 100  $\mu\text{m}$ ). Here, the droplet generation and the breakup process would affect the same flow rate ratio 0.2 in the smaller width of the continuous phase channel, affecting droplet generation with changes of the dispersed phase. A higher width of dispersed channel

(100  $\mu\text{m}$ ) generated a larger droplet compared with a lower width of dispersed channel (50  $\mu\text{m}$ ) with a constant flow ratio (0.2). The droplet size also decreased, and the droplet generation frequency increased by around three times, as shown in Figs. 10 (c) and 10 (d).

Additionally, the pressure difference between P1 and P2, and effective droplet diameter were compared with different geometrical models and flow rates. All geometry profiles produced constant droplet generation, with the exception of Gem-D, which produced unequal intervals of droplet frequency. The pressure difference comparison explained the time gap between the droplet generating process. In this manner, Gem-C had a higher droplet generation than with the other geometries. This means flow rate and geometry affects droplet frequency significantly, as shown in Fig. 11. Figure 12 illustrates the effective diameter of droplets of different geometrical sizes. This comparison shows that reducing the size of the continuous phase width will affect droplet generation. The first and second droplets start the cycle, and each alternative two droplets form a cycle, because the first droplet is bigger than the second. The same phenomena occur repeatedly, as shown in Fig. 12.

##### 4.2.1. Flow rate

In this simulation showed the behavior of droplet generation based on the different flow rate ratios of continuous and dispersed phase flows in the T-junction channel. The flow rate of the dispersed phase flow was constant ( $Q_d = 0.2 \text{ mL/h}$ ), while the continuous phase flow was varied ( $Q_c = 0.2 \text{ to } 4 \text{ mL/h}$ ), and other fluid and physical parameters were constant, such fluid viscosity, wall wetted angle, and density, as based on Table 2. In this, flow ratios were 1, 0.5, 0.2, 0.1, and 0.05.

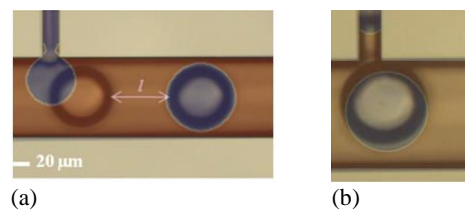


**Fig. 9. Comparison of predicted balloon droplet with experimental results and simulation results: (a) position and shape (b) size.**

**Table 3 Physical properties of fluids (Experiment 2; Tarchichi *et al.* 2013)**

Parameters	Continuous phase	Dispersed phase
Viscosity (Pa. s)	1e-3	41e-3
Density (kg/m <sup>3</sup> )	1e3	1.07e3
Surface tension (N/m)	10e-3	10e-3
Wetted wall contact angle (Deg)	180	180

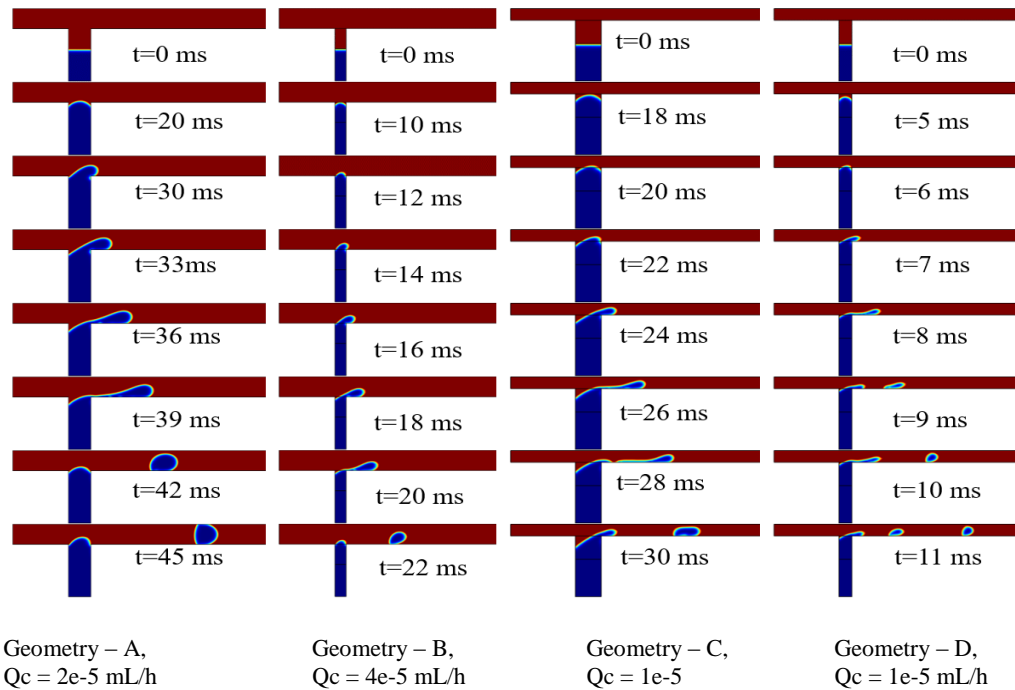


**Fig. 10.** Dissimilar sizes of T-shaped geometrical models for droplet formation with variable continuous phase and constant dispersed flow rate ( $2e-5$  mL/h).

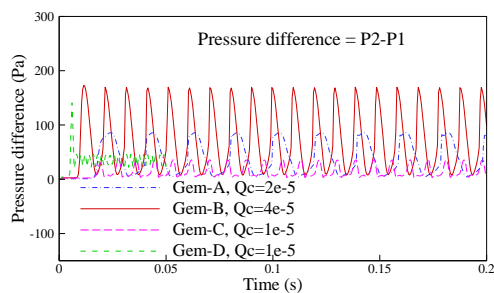


**Fig. 11.** Comparison of pressure difference for dissimilar sizes of T-shaped geometry.

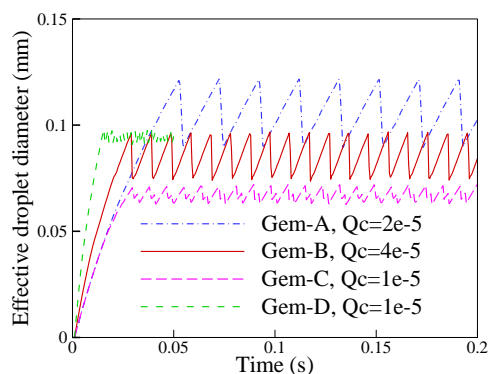


**Fig. 12.** Effective droplet diameter for dissimilar sizes of T-shaped geometry with constant dispersed flow rate.

Figures 13 and 14 illustrate the droplet generation process based on different flow rate ratios from 0.05 to 0.2. Owing to the continuous phase of the viscous shear force and the dispersed phase pressure

variation before entering the continuous phase and after, droplets are detached from the dispersed phase and flow in the main channel along with the continuous phase. Furthermore, when changing the flow ratio, due to the constant value of surface tension, phase density, phase viscosity, and dispersed phase flow, the continuous phase flow rate changed accordingly in the main channel. In the droplet formation process, because of the higher rate of continuous phase in the channel, the viscous shear force increased. Due to this fluid behavior in the channel, the droplets simply and smoothly detached from the dispersed phase and the droplet breakup time as well as the effective diameter also reduced. Increasing the continuous flow rate led to an increase in the droplet generating frequency, and the droplet size and shape were affected. At a lower flow rate of continuous phase below 1ml/h, on the other hand, no droplet was generated, and a slug flow was created in the main channel, as shown in Fig. 13 (a).

#### 4.2.2. Contact angle

Wall surface conditions have a major role in the droplet generating process. Because wall wettability is directly connected with surface properties, it affects droplet generation. The characteristics of the contact angle are decided by the interface between the droplet and the channel wall. The droplet generation method is influenced by it, as it involves the simplicity of droplet generation, and with the droplets spreading into a stream and affects their droplet shape. Consequently, the behavior of a wetted wall microchannel was investigated through modification of the contact angle. A contact angle is the point between the phase interface and the solid wall at the position where the fluid interface connects to the solid wall in COMSOL 5.6. The fluid flow in

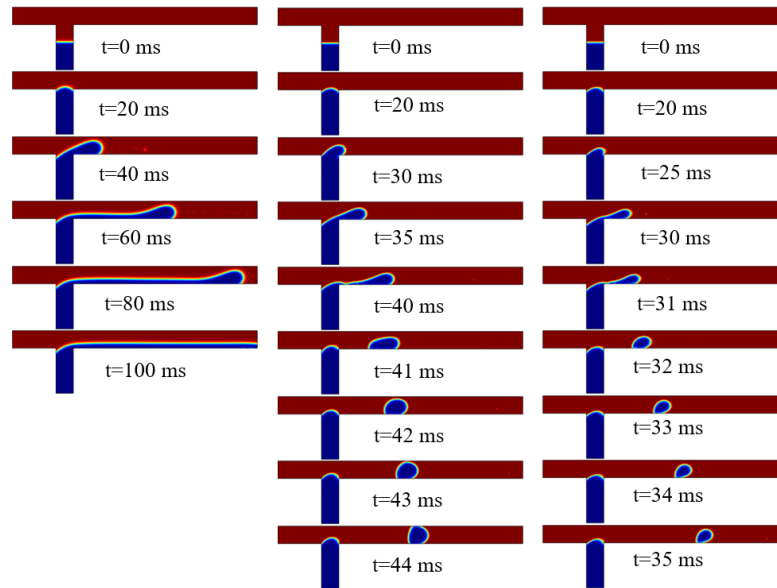


**Fig. 13.** Comparison of droplet generation behavior for different continuous phase flow rate ( $Q_c$ ) and constant dispersed phase flow rate ( $Q_d = 0.2$  mL/h) in Geometry A (T-shaped).

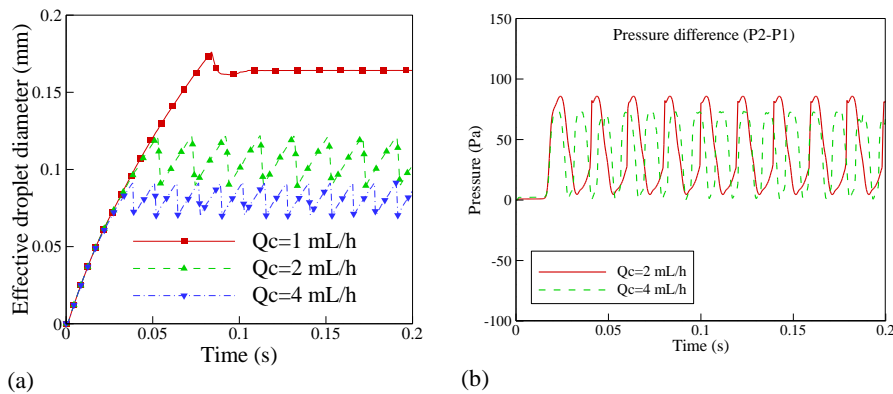


**Fig. 14.** Droplet generation process for different continuous phase flow rate ( $Q_c$ ) and constant dispersed phase flow rate ( $Q_d = 0.2$  mL/h) in Geometry A: (a) effective droplet diameter, and (b) pressure difference.

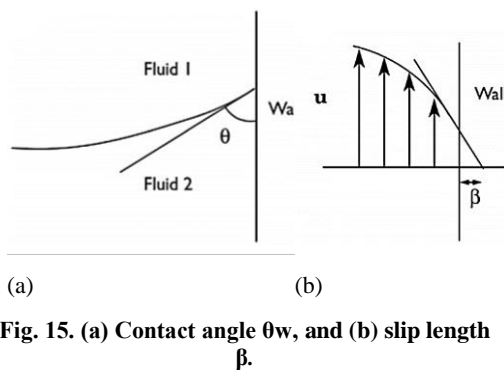


**Fig. 15.** (a) Contact angle  $\theta_w$ , and (b) slip length  $\beta$ .

the confined domain will affect the flow due to slip behavior between the fluid and the solid interface, which is an extended distance relative to the wall where the contact velocity component disappears. This phenomenon of contact angle and velocity slip is graphically explained in Fig. 15. Generally, in the experiments, a wetted wall treated as surface

roughness using a chemical process ensured the wettability at the level of micro/nano structure. In the ensuing numerical analysis, the influence of wall wettability on droplet formation, to predict the minimum of optimal contact angle generating the droplet, was tested using five different contact angles ( $60^\circ$ ,  $90^\circ$ ,  $120^\circ$ ,  $135^\circ$ , and  $180^\circ$ ). Fluid properties and flow rate were kept similar to the validation case.

Figure 16 shows the comparison of droplet generation with different contact angles from  $90^\circ$  to  $180^\circ$ . With increasing contact angle, the effective droplet diameter as well as the droplet volume reduced. Due to the increasing contact angle, the fluid and solid interfacial connection were affected, and there was a decrease in the roughness on the wall; this caused a reduction in wall resistance. With the increasing angle, the droplet generation frequency increased with decreasing volume of droplet formed by equal intervals of generated droplet.

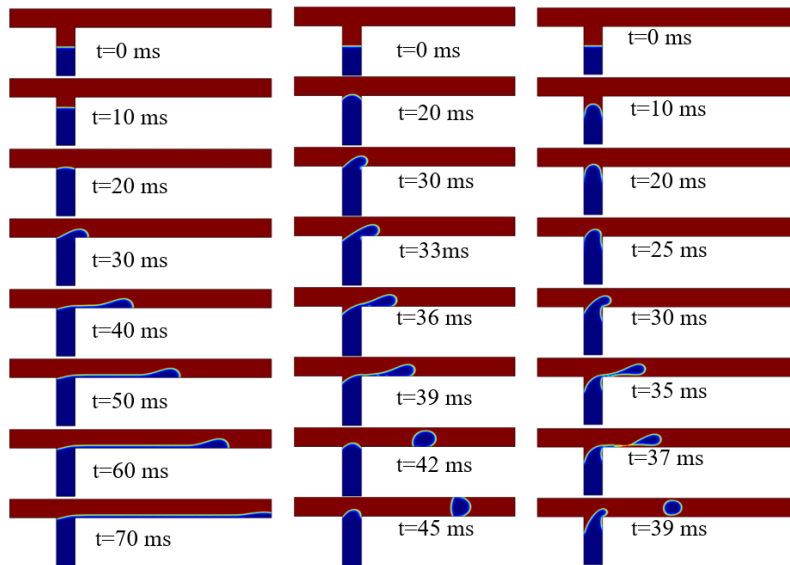


**Fig. 16. Comparison of droplet generation behavior for constant flow rates ( $Q_c = 2 \text{ mL/h}$  and  $Q_d = 0.2 \text{ mL/h}$ ) with different contact angles for Geometry A (T-shaped).**

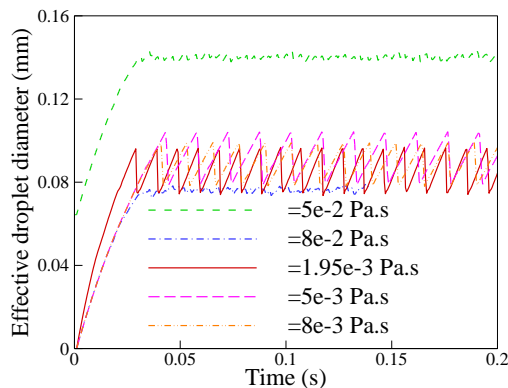


**Fig. 17. Comparison of droplet generation behavior for constant flow rates ( $Q_c = 2 \text{ mL/h}$  and  $Q_d = 0.2 \text{ mL/h}$ ) with different viscosity of continuous phases for Geometry A (T-shaped).**

#### 4.2.3. Viscosity and surface tension

The purpose of this next simulation was to examine the importance of the continuous phase viscosity on the droplet generation process, as shown in Fig. 17. We chose five variations of continuous phase viscosity for this study:  $5e-2$ ,  $8e-2$ ,  $1.95e-3$ ,  $5e-3$ , and  $8e-3$ . The estimate showed that the effective droplet diameter decreased when the viscosity of the continuous phase increased, but when the viscosity of the continuous phase decreased, certain continuous, scattered or cloud droplets were generated in the channel. However, increasing the viscosity indicated a decreasing of droplet diameter. An increase in viscosity caused droplet formation to increase with the effect of viscous shear force. Consequently, droplet breakup developed more quickly, and droplet growth became shorter.

This simulation investigated the two phases of different surface tension behaviors for droplet formation in the microchannel. For the analysis, flow and physical properties, including viscosity, flow rate, density, and channel width were kept constant

for both phases. For testing the surface tension behavior, three different values were considered. From the experimental value, higher and lower conditions were selected for the simulation, such as  $4e-3$ . The optimal conditions to generate a droplet are provided by  $5e-3$  and  $10e-3 \text{ N/m}$ . Figure 18 shows the comparison of different surface tensions. When there is a decrease of surface tension, after a certain time, droplets will not be generated; instead a slug forms in the channel. But by increasing the surface tension, the droplet will form continuously, with a gradually elongated droplet being generated, as shown in Fig. 18.

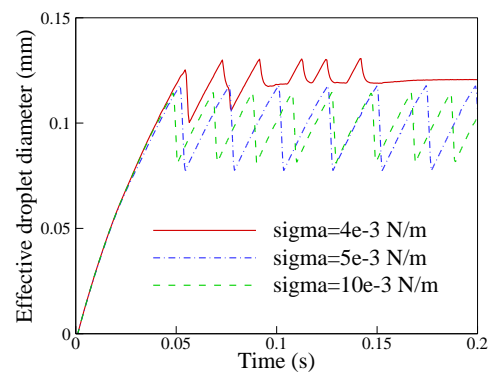


**Fig. 18. Comparison of droplet generation behavior for constant flow rates ( $Q_c = 2 \text{ mL/h}$  and  $Q_d = 0.2 \text{ mL/h}$ ) with different surface tension of between two immiscible fluids for Geometry A (T-shaped).**

#### 4.3. Distributor Influence

In this simulation, details of different types of distributors and optimal flow rate to generate droplets are elucidated. Slug flow behavior was not considered. We made a numerous simulation to predict the optimal flow ratio of the continuous phase and dispersed phase. Initially, we considered a

continuous phase flow rate ( $Q_c$ ) of  $2e-6$  mL/h and a dispersed phase flow rate ( $Q_d$ ) of  $0.2e-6$ ; a ratio of  $Q_d/Q_c = 0.1$  was an optimal ratio to verify the different distributor geometry. From Section 4.1, the flow rate ratio of 0.1 provided a good prediction of testing different geometry droplet behavior. This flow ratio was used to predict the droplet shape and generating frequency under different geometrical shapes, including forward and backward inclined webs with different angles ( $30^\circ$ ,  $45^\circ$ , and  $60^\circ$ ), L-junction, and Y-junction with different angles ( $30^\circ$ ,  $45^\circ$ , and  $60^\circ$ ). These geometries were compared with the T-junction effective droplet diameter, pressure difference P3-P1, and P3 pressure.

The various types of structured distributor geometries were tested for their droplet generation behavior. This was dependent on the dispersed phase channel meeting the continuous phase channel. Droplet size, shape, and flow behavior changed. First in the discussion is about webs inclined backward dispersed flow channel, as shown in Fig. 2 (a). When the position of the webs are in a backward angle of attack, the channel angle seems opposite to the flow direction continuous flow. Thus, the shear force is high when the dispersed phase meets the continuous phase. Due to this shear angle change, the droplet generation rate is significantly affected. The droplet generation occurred after a certain flow ratio, such as 0.1. When the flow ratio ( $Q_d/Q_c$ ) increased, instead of droplet generation, a Taylor bubble, discontinued bubble, or slug was generated depending on the flow ratio. However, here we address the droplet formed in the 0.1 flow ratio. The changes of the dispersed phase angle would not affect the droplet shape, but the droplet generation ratio was affected, as shown in Fig. 19.

On the other hand, Fig. 20 shows the forward inclined webs with different angles. In the geometry, webs in a forward inclined position between a continuous phase and a dispersed shear force have a low angle because of the flow vector of the dispersed phase toward the continuous phase flow vector direction. As a result, when two flows meet at the junction, the shear force is lower than the T-junction geometry. In this type of geometry, a low flow ratio operates compared with the T-junction. The minimum flow ratio of droplet generation was 0.05 when the flow ratio was increased; this affects droplet generation, and it generates the slug flow behavior due to the low shear force. Even with a decrease of the web channel angle, the droplet generation rate as well as the droplet breakup are affected. This is because the shear force reduces while the angle decreases, as shown in Fig. 20.

Figure 21 shows a comparison of the Y-junction with different angles of continuous and dispersed flow channels. The present geometry is completely different from forward and backward inclined web geometries. In this geometry, both phase channels inclined towards each other. The channel angle is measured at the mid-axis of the main channel. Due to both channels being inclined at the same angle, the vector of flow direction of both channels collides at the junction. Owing to this behavior, the flow rate

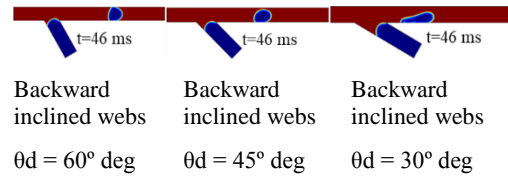


**Fig. 19. Comparison of droplet generating behavior for backward inclined webs with different angles of dispersed channels using constant flow rates ( $Q_c = 2$  mL/h and  $Q_d = 0.2$  mL/h).**

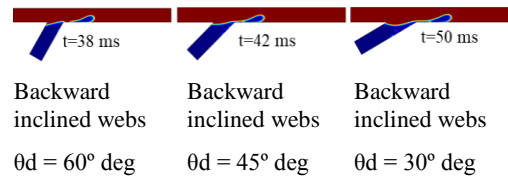


**Fig. 20. Comparison of droplet generating behavior for forward inclined webs with different angles of dispersed channels using constant flow rates ( $Q_c = 2$  mL/h and  $Q_d = 0.2$  mL/h).**

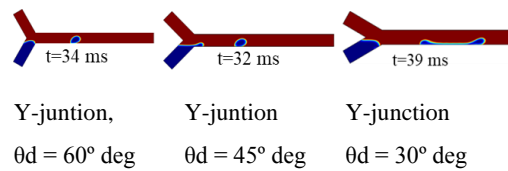


**Fig. 21. Comparison of Y-junction with different angle under ( $Q_c = 2$  mL/h and  $Q_d = 0.2$  mL/h).**

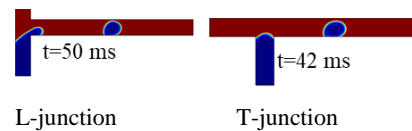


**Fig. 22. Comparison of L- and T- junction under ( $Q_c = 2$  mL/h and  $Q_d = 0.2$  mL/h).**

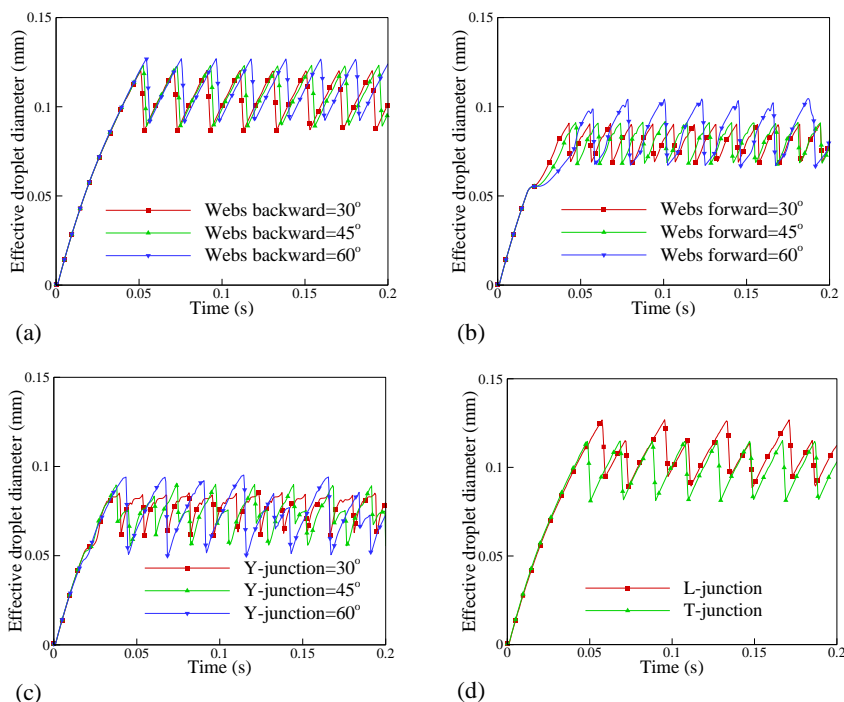
and viscosity majorly influenced the droplet generation process. When the flow ratio was approximately above 0.05, instead of droplet generation, long bubbles or slugs formed. Furthermore, by reducing the angle, the droplet process will change continuously with the angle of the channel, as shown in Fig. 21. The generated droplet shape and size were affected with respect to the angle. As the angle neared  $30^\circ$ , an elongated droplet was generated from the breakup, and then it changed to a circular droplet. During this process, the droplet exhibited elastic flow and it caused back pressure to be created in the channel.

Figure 22 shows the L- and T-junction geometry generated droplets at the flow ratio of 0.1. The L-junction geometry arrangement has both channels fixed on the same axis, meaning the flow vectors are directly opposite one another. Both channels are connected to the main channel at  $90^\circ$ . The simulation results of L-shape geometry compared the T-junction

with same flow condition of T-junction. The droplet shape and size were affected due to the high-impact force on the dispersed phase from the continuous phase at the L-junction, and this affected droplet shape and size. However, the droplet processes of pinch off and breakup took longer because of strong interfacial tension near the wall of the main channel connected to the phase channels.

Figure 23 compares the different geometrical models with their generated droplet size and frequency of droplet. Clearly, when the model is changed, the droplet size, shape, and frequency will be affected, but such changes need to be understood for the purpose of being able to design better microdevices. In this way, while comparing different geometrical

droplet diameters and frequencies, we observed significant changes due to the geometrical shape, angle of geometry, and operating flow ratio. Figures 23 (a) and 23 (d) show a similar profile, with the droplet generation process occurring in a linear manner, compared with the other geometries. In Fig. 23 (a), the decreasing of web angle droplet diameters reduces and the bubble frequency level increases according to the geometry. Figure 23 (d) shows the different droplet frequency and diameter of the L-junction geometry. The droplet makes a pair set, with the first droplet being higher and the second droplet being smaller. This action repeatedly occurs until 0.2s, and these kinds of geometries helped to generate alternative processes.



**Fig. 23. Comparison of effective droplet diameter with various types of microdroplet generator/distributor.**

Furthermore, Figs. 23 (b) and 20 (c) show a similar kind of profile. In the frequency profile, the droplet generating process is affected during the stages of blocking, pinch off, and breakup. Figure 23 (b) shows that changes to the web forward angle affect the droplet process as well as droplet size; a different profile is formed compared with Fig. 23 (a). Figure 23 (c) shows the Y-junction droplet profile. It clearly shows that increasing the channel angle increases the droplet diameter, and that droplet frequency decreases.

### 5. INFLUENCE OF SPLITTER/BREAKER

Droplet splitting is a pioneering technique for increasing the efficiency of a reaction depending on the microfluidic approach. The technique has been adopted in most microfluidic processing industries, including for use in chemical kinetic reactions and

the pharmaceutical industry. In this simulation took a constant flow ratio of 0.1, and a droplet was generated from a T-junction and passed through a splitter domain. The droplet from the T-junction resembled a bullet shape and flowed symmetrically in the main channel. The splitter geometrical model was considered as a symmetrical flow divider. Most previous work considered a single droplet splitting mechanism from a mother droplet to two sister droplets, but here we have discussed generating the mother droplet and splitting the droplet using different types of splitters. For this simulation we considered five different types of splitting geometrical designs and compared the pressure behavior at the symmetrical position of splitter. The geometries were V-shaped with different angles, H-shaped, needle, M-shaped, and root-shaped. The simulation took a 0.1 flow ratio for all models and calculated a computational time of 0.2 s.

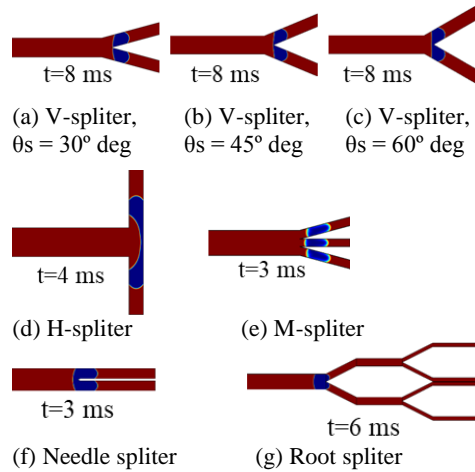


**Fig. 24. Comparison of Y-junction with different angle under ( $Q_c = 2 \text{ mL/h}$  and  $Q_d = 0.2 \text{ mL/h}$ ).**

Figures 3(a) – (d) show the different types of splitting geometries. The mother droplet comes from the T-junction as the droplet generator to the splitter. The two-channel inner wall connects each other and forms a splitting edge, and the outer wall connects with the main channel with a certain position or angle. The inner edge position is the droplet-hitting position, and the droplet pressure increases at the nose. Furthermore, the droplet penetrating the splitter will be divided symmetrically into two droplets. This phenomenon changes the mother droplet into two sister droplets. An increase in the V-shaped splitter angle leads to an increase in the droplet splitting time, as shown in Fig. 24 (a) – (c).

Figure 24 (d) shows the impact of a droplet divided into two droplets. The two splitting channels are connected with the main channel at a  $90^\circ$  angle, and two dividing channels are connected in the line of the axis at  $180^\circ$ . In this geometry there is no connecting shape edge. However, the incoming droplet in the main channel directly hits the middle of the two splitting channels and divides into two separate droplets. This separation mechanism highly depends on the continuous phase flow rate; a higher flow rate sees droplet splitting occurring more quickly than with a low flow rate. This system is quite different from the rest of the model.

Figure 24 (e) shows the M-shaped droplet splitting geometry. The purpose of this geometry is to generate a greater number of droplets from the mother droplet. Generally, the middle of the droplet volume is higher than the top and bottom of the droplet, so the splitter to divided ratio is taken as  $3.5 : 3 : 3.5$ , forming the M-shaped droplet. The volume of the separated three parts are nearly same. This droplet looks like a Taylor droplet, and it occupies both ends of the wall. This geometry has three different channels to flow through the droplet

Figure 24 (f) shows the needle-type splitting method. Near the exit of the main channel, the channel is split into a thin layer placed in the middle of the main channel. Geometrically, it looks like two different channels inside the main channel. When the droplet nose meets the needle edge, pressure increases at the

needle edge and breaks the surface tension; the mother droplet becomes separated into two different droplets. In this geometry, the narrow type of droplet-splitting method was defined and was much completed from the design aspect. The tree root channel based on multiple V-shapes was attached at each outlet port and formed the root. Continuous droplet splitting seemed to occur in a chain, branch by branch. This kind of geometry produces a smaller droplet than is produced by the distributor. A root-shaped splitter helps to mix two or more different materials together showed in Fig. 24 (g).

## 5. CONCLUSION

This numerical investigation of microdroplet generation and break up with different geometrical model structures in immiscible fluid (water and oil) phases was accomplished with use of COMSOL 5.6. We validated the droplet generation with two different experimental results in order to improve the numerical model stabilization. The implemented simulation setup predictions for the droplet size, position, frequency, and shape were compared with experimental results. The results of the present simulation are in good agreement with the experimental results. The generation of the droplet process was examined until 0.2 s, in which time approximately 8–20 microdroplets were generated. With this, the study focused on the different fluid conditions, different physical properties and geometry of the droplet generator and splitter to predict the optimal conditions for generating droplets. From the numerical simulation results, the completion of the droplet generation process and the droplet splitter can be summarized as follows.

Droplet frequency generation was based on increasing the continuous flow rate and contact angle, and also on decreasing the channel width. In contrast, the decreasing of flow rate and contact angle led to a continuous slug being created in the main channel and the interaction between the dispersed phase and the solid wall reducing near the junction. This was due to droplet break up occurring earlier in higher contact angle while the droplet breakup is delayed in in the lower contact angle. Furthermore, a change of viscosity in the continuous phase, and the interfacial force, affected droplet generation due to the sensitivity of fluid viscosity.

The droplet formation purely depends on the structure of the geometrical shape, size, and channel angle. The T-junction and backward inclined web channel could generate larger droplets, and smaller droplets could be generated by lower angle geometry, such as Y-junction  $30^\circ$  and forward inclined web  $30^\circ$ .

In droplet splitting technique, based on the shape of the splitting edges and the output channel shape arrangements and increasing of splitter angle, could significantly increase the splitting frequency. We simulated an effective splitting technique to produce microdroplets. Based on the splitting technique, the two-droplet approach involved V-shaped, needle, and H-shaped, and the three-droplet approach

involved an M-shaped splitter; for more droplets, a root-shape can be used.

Future work should investigate synchronous and asynchronous droplet formation in double T-junction geometry.

#### ACKNOWLEDGEMENTS

This work was supported by the Hydrogen Energy Innovation Technology Development Program of the National Research Foundation of Korea (NRF) funded by the Korean government (Ministry of Science and ICT (MSIT)) (NRF-2019M3E6A1064290) and by the National Research Foundation of Korea (NRF) grant funded by the Korea government (NRF- 2019M1A2A2065614).

#### REFERENCES

- Ba, Y., H. Liu, J. Sun and R. Zheng (2015). Three dimensional simulations of droplet formation in symmetric and asymmetric T-junctions using the color-gradient lattice Boltzmann model. *International Journal of Heat and Mass Transfer* 90, 931-947.
- Chen, D. L., C. J. Gerdtts and R. F. Ismagilov (2005). Using Microfluidics to Observe the Effect of Mixing on Nucleation of Protein Crystals. *Journal of the American Chemical Society* 127(27), 9672-9673.
- Chen, H., Q. Fang, X. F. Yin and Z. L. Fang (2005). Microfluidic chip-based liquid-liquid extraction and preconcentration using a subnanoliter-droplet trapping technique [10.1039/B416964F]. *Lab on a Chip* 5(7), 719-725.
- Chen, Y. S., Y. L. Huang, C. H. Kuo and S. H. Chang, (2007). Investigation of design parameters for droplet generators driven by piezoelectric actuators. *International Journal of Mechanical Sciences* 49(6), 733-740.
- Cybulski, O., P. Garstecki and B. A. Grzybowski (2019). Oscillating droplet trains in microfluidic networks and their suppression in blood flow. *Nature Physics* 15(7), 706-713.
- Dittrich, P. S. and A. Manz (2006). Lab-on-a-chip: microfluidics in drug discovery. *Nature Reviews Drug Discovery* 5(3), 210-218.
- Gach, P. C., K. Iwai, P. W. Kim, N. J. Hillson and A. K. Singh (2017). Droplet microfluidics for synthetic biology [10.1039/C7LC00576H]. *Lab on a Chip* 17(20), 3388-3400.
- Garstecki, P., H. A. Stone and G. M. Whitesides (2005). Mechanism for flow-rate controlled breakup in confined geometries: a route to monodisperse emulsions. *Physical Review Letters* 94(16), 164501.
- Han, W. and X. Chen (2021). A review on microdroplet generation in microfluidics. *Journal of the Brazilian Society of Mechanical Sciences and Engineering* 43(5).
- Hatakeyama, T., D. L. Chen and R. F. Ismagilov (2006). Microgram-Scale Testing of Reaction Conditions in Solution Using Nanoliter Plugs in Microfluidics with Detection by MALDI-MS. *Journal of the American Chemical Society* 128(8), 2518-2519.
- Hong, Y. and F. Wang (2007). Flow rate effect on droplet control in a co-flowing microfluidic device. *Microfluidics and Nanofluidics* 3(3), 341-346. <https://doi.org/10.1007/s10404-006-0134-3>
- Joanicot, M. and A. Ajdari (2005). Droplet Control for Microfluidics. *Science* 309 (5736), 887.
- Jung, J. H., G. Destgeer, B. Ha, J. Park and H. J. Sung (2016). On-demand droplet splitting using surface acoustic waves [10.1039/C6LC00648E]. *Lab on a Chip* 16(17), 3235-3243.
- Kim, L. S., H. K. Jeong, M. Y. Ha and K. C. Kim (2008). Numerical simulation of droplet formation in a micro-channel using the lattice Boltzmann method. *Journal of Mechanical Science and Technology* 22(4), 770-779.
- Liu, H. and Y. Zhang (2009). Droplet formation in a T-shaped microfluidic junction. *Journal of Applied Physics* 106(3), 034906.
- Luo, J., S. Y. Wu, L. Xiao and Z. L. Chen (2021). Parametric influencing mechanism and control of contact time for droplets impacting on the solid surfaces. *International Journal of Mechanical Sciences* 197, 106333.
- Madadelahi, M., M. J. Madou, Y. D. Nokoorani, A. Shamloo and S. O. Martinez-Chapa (2020). Fluidic barriers in droplet-based centrifugal microfluidics: Generation of multiple emulsions and microspheres. *Sensors and Actuators B: Chemical* 311, 127833.
- Mastiani, M., B. Mosavati and M. Kim (2017). Numerical simulation of high inertial liquid-in-gas droplet in a T-junction microchannel. *RSC Advances* 7(77), 48512-48525.
- Ngo, I. L., T. D. Dang, C. Byon and S. W. Joo (2015). A numerical study on the dynamics of droplet formation in a microfluidic double T-junction. *Biomicrofluidics* 9(2), 024107.
- Nie, Z., S. Xu, M. Seo, P. C. Lewis and E. Kumacheva (2005). Polymer Particles with Various Shapes and Morphologies Produced in Continuous Microfluidic Reactors. *Journal of the American Chemical Society* 127(22), 8058-8063.
- Olsson, E. and G. Kreiss (2005). A conservative level set method for two phase flow. *Journal of Computational Physics* 210(1), 225-246.
- Osher, S. and R. Fedkiw (1991). *Level Set Methods and Dynamic Implicit Surfaces*. Springer, New York, NY.
- Osher, S. and J. A. Sethian (1988). Fronts propagating with curvature-dependent speed: Algorithms based on Hamilton-Jacobi

- formulations. *Journal of Computational Physics* 79(1), 12-49.
- Raj, R., N. Mathur and V. V. Buwa (2010). Numerical Simulations of Liquid-Liquid Flows in Microchannels. *Industrial & Engineering Chemistry Research* 49(21), 10606-10614.
- Rambach, R. W. K., Linder, M. Heymann and T. Franke (2017). Droplet trapping and fast acoustic release in a multi-height device with steady-state flow [10.1039/C7LC00378A]. *Lab on a Chip* 17(20), 3422-3430.
- Sartipzadeh, O., S. M. Naghib, A. Seyfoori, M. Rahmanian and F. S. Fatemina (2020). Controllable size and form of droplets in microfluidic-assisted devices: Effects of channel geometry and fluid velocity on droplet size. *Materials Science and Engineering: C* 109, 110606.
- Shang, L., Y. Cheng and Y. Zhao (2017). Emerging Droplet Microfluidics. *Chemical Reviews* 117(12), 7964-8040.
- Shestopalov, I., J. D. Tice and R. F. Ismagilov (2004). Multi-step synthesis of nanoparticles performed on millisecond time scale in a microfluidic droplet-based system [10.1039/B403378G]. *Lab on a Chip* 4(4), 316-321.
- Shi, Y., G. H. Tang and H. H. Xia (2014). Lattice Boltzmann simulation of droplet formation in T-junction and flow focusing devices. *Computers & Fluids* 90, 155-163.
- Shum, H. C., A. Bandyopadhyay, S. Bose and D. A. Weitz (2009). Double Emulsion Droplets as Microreactors for Synthesis of Mesoporous Hydroxyapatite. *Chemistry of Materials* 21(22), 5548-5555.
- Song, H., J. D. Tice and R. F. Ismagilov (2003). A Microfluidic System for Controlling Reaction Networks in Time *Angewandte Chemie International Edition* 42(7), 768-772.
- Srikanth, S., S. K. Dubey, A. Javed and S. Goel (2021). Droplet Based Microfluidics Integrated with Machine Learning. *Sensors and Actuators A: Physical*, 113096.
- Tarchichi, N., F. Chollet and J. F. Manceau (2013). New regime of droplet generation in a T-shape microfluidic junction. *Microfluidics and Nanofluidics* 14(1), 45-51.
- Thorsen, T., R. W. Roberts, F. H. Arnold, F. H. and S. R. Quake (2001). Dynamic pattern formation in a vesicle-generating microfluidic device. *Physical Review Letters* 86(18), 4163-4166.
- Um, E., M. Kim, H. Kim, J. H. Kang, H. A. Stone and J. Jeong (2020). Phase synchronization of fluid-fluid interfaces as hydrodynamically coupled oscillators. *Nature Communications* 11(1), 5221.
- Utada, A. S., A. Fernandez-Nieves, H. A. Stone and D. A. Weitz (2007). Dripping to jetting transitions in coflowing liquid streams. *Physical Review Letters* 99(9), 094502.
- van der Graaf, S., T. Nisisako, C. G. P. H. Schroën, R. G. M. van der Sman and R. M. Boom (2006). Lattice Boltzmann Simulations of Droplet Formation in a T-Shaped Microchannel. *Langmuir* 22(9), 4144-4152.
- Venkateshwarlu, A. and R. P. Bharti (2021). Effects of capillary number and flow rates on the hydrodynamics of droplet generation in two-phase cross-flow microfluidic systems. *Journal of the Taiwan Institute of Chemical Engineers* 139, 64-79
- Yang, C. G., Z. R. Xu and J. H. Wang (2010). Manipulation of droplets in microfluidic systems. *TrAC Trends in Analytical Chemistry* 29(2), 141-157.
- Yang, Q., D. Ju, Y. Liu, X. Lv, Z. Xiao, B. Gao, F. Song and F. Xu (2021). Design of organ-on-a-chip to improve cell capture efficiency. *International Journal of Mechanical Sciences* 209, 106705.
- Yen, B. K. H., A. Günther, M. A. Schmidt, K. F. Jensen and M. G. Bawendi (2005). A Microfabricated Gas-Liquid Segmented Flow Reactor for High-Temperature Synthesis: The Case of CdSe Quantum Dots *Angewandte Chemie International Edition* 44(34), 5447-5451.
- Zeng, W., Z. Tong, X. Shan, H. Fu and T. Yang (2021). Monodisperse droplet formation for both low and high capillary numbers in a T-junction microdroplet generator. *Chemical Engineering Science* 243, 116799.
- Zhang, J., W. Xu, F. Xu, W. Lu, L. Hu, J. Zhou, C. Zhang and Z. Jiang (2021). Microfluidic droplet formation in co-flow devices fabricated by micro 3D printing. *Journal of Food Engineering*, 290, 110212.
- Zhang, K., Q. Liang, S. Ma, X. Mu, P. Hu, Y. Wang and G. Luo (2009). On-chip manipulation of continuous picoliter-volume superparamagnetic droplets using a magnetic force [10.1039/B906229G]. *Lab on a Chip* 9(20), 2992-2999.
- Zhang, Z., J. Zhao, X. Ling and J. Ma (2021). Numerical study on dynamic behaviours of a micro-droplet impacting on a vertical wall in PEMFC. *International Journal of Hydrogen Energy* 46(35), 18557-18570.
- Zhu, P., T. Kong, Z. Kang, X. Tian and L. Wang (2015). Tip-multi-breaking in Capillary Microfluidic Devices. *Scientific Reports* 5, 11102.
- Zhu, P. and L. Wang (2017). Passive and active droplet generation with microfluidics: a review [10.1039/C6LC01018K]. *Lab on a Chip*, 17(1), 34-75.